THE JOURNAL OF BIOLOGICAL CHEMISTRY
Vol. 278, No. 34, Issue of August 22, pp. 32107–32114, 2003
Printed in U.S.A.

The Negative Transcriptional Regulator NmrA Discriminates between Oxidized and Reduced Dinucleotides*

Received for publication, April 18, 2003, and in revised form, May 14, 2003
Published, JBC Papers in Press, May 22, 2003, DOI 10.1074/jbc.M304104200

Heather K. Lamb‡§, Kris Leslie§¶, Anna L. Dodds‡, Margaret Nutley‖, Alan Cooper‖, Christopher Johnson‡, Paul Thompson‡, David K. Stammers¶, and Alastair R. Hawkins‡ ‡‡**

From the ‡School of Cell and Molecular Biosciences, Catherine Cookson Building, University of Newcastle upon Tyne, Framlington Place, NE2 4HH, United Kingdom, ¶Division of Structural Biology, The Henry Wellcome Building for Genomic Medicine, University of Oxford, Roosevelt Drive, Oxford OX3 7BN, United Kingdom, and the ‖Department of Chemistry, University of Glasgow, Glasgow G12 8QQ, Scotland, United Kingdom

NmrA, a transcription repressor involved in the regulation of nitrogen metabolism in *Aspergillus nidulans*, is a member of the short-chain dehydrogenase reductase superfamily. Isothermal titration calorimetry and differential scanning calorimetry have been used to show NmrA binds NAD^+ and $NADP^+$ with similar affinity (average K_D 65 μM) but has a greatly reduced affinity for NADH and NADPH (average K_D 6.0 mM). The structure of NmrA in a complex with $NADP^+$ reveals how repositioning a His-37 side chain allows the different conformations of NAD^+ and $NADP^+$ to be accommodated. Modeling NAD(P)H into NmrA indicated that steric clashes, attenuation of electrostatic interactions, and loss of aromatic ring stacking can explain the differing affinities of $NAD(P)^+$/NAD(P)H. The ability of NmrA to discriminate between the oxidized and reduced forms of the dinucleotides may be linked to a possible role in redox sensing. Isothermal titration calorimetry demonstrated that NmrA and a C-terminal fragment of the GATA transcription factor AreA interacted with a 1:1 stoichiometry and an apparent K_D of 0.26 μM. NmrA was unable to bind the nitrogen metabolite repression signaling molecules ammonium or glutamine.

Neurospora crassa, *Aspergillus nidulans*, and other ascomycetous fungi are able to utilize a wide array of nitrogen sources, and many of the pathways involved are regulated at the level of transcription by pathway-specific control proteins. When the preferred nitrogen sources ammonium or glutamine are present in the growth medium with an alternative nitrogen source, the pathway for the non-preferred source remains inactive. This situation is known as nitrogen metabolite repression, and the alternate nitrogen utilization pathway is said to be repressed (1). These observations show there is a signal transduction pathway that responds to the presence of ammonium/glutamine and targets the control of transcription of the genes involved in nitrogen metabolism.

Two major classes of mutant affecting nitrogen metabolite repression have been isolated. The first class exemplified by the *nmr-1* and *nmrA* genes of *N. crassa* and *A. nidulans*, respectively, has a partially de-repressed phenotype (2, 3) implying they act as negative transcription regulators.

The structures of the native form of the *nmrA*-encoded NmrA protein as well as a complex with NAD^+ have been reported (4, 5). Structural comparisons reveal that NmrA shows an unexpected similarity to the short-chain dehydrogenase reductase (SDR) superfamily (5), with the closest relationship to UDP-galactose 4-epimerase (root mean square deviation for 251 equivalent α-carbons of 2.7 Å). Whereas UDP-galactose 4-epimerase has the conserved Tyr-*X*-*X*-*X*-Lys SDR catalytic motif (6, 7), in NmrA this is changed to Met-*X*-*X*-*X*-Lys. The loss of a key catalytic tyrosine implies NmrA is unlikely to be an active dehydrogenase. The N-terminal domain of NmrA consists of a Rossmann fold, which, despite lacking the characteristic nucleotide-binding motif Gly-*X*-*X*-Gly-*X*-*X*-Gly, is able to bind NAD^+ (5). Prior to the structural work on NmrA, NAD^+ binding was an unreported property of the protein that could not be predicted from bioinformatics or genetic studies. However, in order to assess the possible physiological significance of such binding, it is necessary to characterize the relative strength of NAD^+ as well as $NADP^+$ binding to NmrA in both their oxidized and reduced forms.

The *nit-2* and *areA* genes that encode the GATA-binding NIT2 and AreA proteins of *N. crassa* and *A. nidulans*, respectively, exemplify the second class of mutants. These proteins contain single zinc fingers and are required to stimulate transcription of genes controlled by nitrogen metabolite repression (8–12). Loss of function mutants are unable to use non-preferred nitrogen sources and are said to have a repressed phenotype in contrast to the wild-type repressible phenotype.

The molecular mechanism of the signal transduction pathway responsible for nitrogen metabolite repression is complex and in *A. nidulans* includes control of mRNA stability mediated through the 3′-untranslated region of the *areA* mRNA and AreA-dependent re-modeling of chromatin domains (13, 14). *In vivo* post-translational modulation of NIT2 activity has been implicated, as *in vitro* the *nmr1*-encoded N-terminally deleted forms of NMR1 protein bind directly to the zinc finger region and the extreme C-terminal 30 amino acids of NIT2 (15–17). The interactions were demonstrated in a qualitative manner by using the yeast two-hybrid system, as well as steady state techniques that included electrophoretic mobility shift assay and column binding using His_6- and glutathione *S*-transferase-tagged fragments of the NIT2 protein as a bait. No kinetic data nor the strength of the interaction with the wild-type NMR1 have been reported. Here we investigate the ligand binding

* This work was supported by the Biotechnology and Biological Sciences Research Council and the Wellcome Trust. The costs of publication of this article were defrayed in part by the payment of page charges. This article must therefore be hereby marked "*advertisement*" in accordance with 18 U.S.C. Section 1734 solely to indicate this fact.

The atomic coordinates and structure factors (code 1PDS) have been deposited in the Protein Data Bank, Research Collaboratory for Structural Bioinformatics, Rutgers University, New Brunswick, NJ (http://www.rcsb.org/).

§ Both authors contributed equally to this work.

** To whom correspondence may be addressed. Tel.: 44-1865-287-565; Fax: 44-1865-287-547; E-mail: daves@strubi.ox.ac.uk.

‡‡ To whom correspondence may be addressed. Tel.: 44-191-2227673; Fax: 44-191-2227424; E-mail: a.r.hawkins@ncl.ac.uk.

properties of NmrA and show that it binds to a C-terminal fragment of AreA, the dinucleotides NAD^+ and $NADP^+$, but not their reduced forms, and not to the nitrogen metabolite signal molecules ammonium and glutamine. These properties of NmrA suggest a possible link to a redox-sensitive signal transduction pathway.

EXPERIMENTAL PROCEDURES

Materials—Chemicals and solvents were purchased from local suppliers and were of AnalaR or greater purity. Enzyme substrates were purchased from Sigma, and molecular biology reagents (which were used in accordance with the manufacturers recommendations) were purchased from Invitrogen, Amersham Biosciences, BCL, or the University of Newcastle upon Tyne Facility for Molecular Biology.

Molecular Biology and Biochemistry—Routine molecular biology protocols followed individual manufacturer's recommendations or were as described previously (18, 19). All DNA sequencing was carried out on double-stranded plasmid DNA using an ABI PRISM 377 DNA sequencer in the University of Newcastle upon Tyne Facility for Molecular Biology.

Construction of a Recombinant Plasmid for Expression in Escherichia coli—The *areA* deletion mutant $areA_{662}$ was amplified by the PCR using 5′ sense oligonucleotides (containing an *Nco*I recognition site) of sequence CCAGTCCAGGCGCCATGGAGAACGGAGAGC and a 3′ antisense oligonucleotide (containing a *Hin*dIII site) of sequence CTTTAGAAGCTTACAAACTCA. The PCR used the following conditions: cycle 1–94 °C for 2 min, 50 °C for 2 min, 72 °C for 4 min; cycles 2–30 at 94 °C for 1 min, 50 °C for 2 min, and 72 °C for 4 min using "Expand" high fidelity *Taq* polymerase (Roche Applied Science). After suitable digestion, the DNA sequence was subcloned into the *E. coli* expression vector pRSETB (Invitrogen) placing it under the control of the isopropyl-1-thio-β-D-galactopyranoside-inducible T7 promoter. This plasmid was designated pRF48.

Overproduction and Purification of the $AreA_{662}$ Protein—500-ml cultures of *E. coli* strain BL21DE3 pLysS containing plasmids pRF48 were grown to an attenuation (D_{500}) of 0.2 in rich medium at 37 °C in the presence of 50 μg of ampicillin ml^{-1} and 35 μg ml^{-1} chloramphenicol when 0.2 mg of isopropyl-1-thio-β-D-galactopyranoside ml^{-1} was added, and growth was continued for a further 4 h. After harvesting by centrifugation, the cell pellets were resuspended in 40 ml of 50 mM potassium phosphate, pH 7.2, 0.5 M NaCl, 1 mM DTT,[1] 1 mM benzamidine (buffer 1), and following sonication a cell-free extract was prepared by centrifugation at 2,500 × *g* for 30 min at 4 °C. Proteins in the sonicate capable of zinc binding were adsorbed onto a 27.15-ml chelating Sepharose column that had been charged to one-third capacity with zinc and equilibrated in buffer 1. Loosely bound proteins were eluted from the column with a 100-ml step wash of buffer 1 containing 2.0 M glycine. Tightly bound proteins were then eluted with a 50 mM potassium phosphate linear 6.0 to 4.0 pH gradient containing 0.5 M NaCl and 1 mM DTT, and AreA-containing fractions were identified by SDS-PAGE and pooled. The pooled fractions were dialyzed overnight at 4 °C against 5 liters of buffer containing 50 mM potassium phosphate, 0.5 M KCl, 1 mM DTT, 10 μM $ZnSO_4$, pH 7.2, and subsequently concentrated 2–5-fold by pressure concentration using argon and a ChemLab concentrator in conjunction with a YM10 DIAFLO ultrafiltration membrane.

Purification of NmrA—NmrA was purified using the protocol described previously (4).

Circular Dichroism and Fluorescence Spectroscopy—The secondary structure of NmrA was probed by far-UV CD and the tertiary structure by near-UV CD spectroscopy. CD spectra were recorded from five accumulative scans at 20 °C using a Jobin-Yvon CD6 spectrometer (Longjumeau, France). Samples of NmrA in 50 mM KPO_4, pH 7.4, were used at concentrations between 0.57 and 0.78 mg ml^{-1}. Each spectrum was corrected by subtraction of a comparative blank, and the readings were repeated in the presence of 2.0 mM ammonium chloride or glutamine.

Fluorescence emission spectra were recorded at 20 °C in an SLM 8100 spectrofluorometer operating in ratio mode with bandwidths of 8 mm for excitation (280 and 295 nm) and emission (range 295–430 nm); 5-mm pathlength quartz cuvettes (Hellma) were used containing 500 μl of sample in 50 mM KPO_4, pH 7.4. Samples of NmrA in 50 mM KPO_4, pH 7.4, were used at concentrations between 41 and 46 μg ml^{-1}, and the readings were repeated in the presence of 2.0 mM ammonium chloride or glutamine.

Isothermal Titration Calorimetry—Isothermal titration calorimetry experiments at 25 °C were performed using a high precision VP-ITC system (Microcal Inc.). For potential small effector molecule binding studies, NmrA in the calorimetric cell (1.4 ml) in the range 80–163 μM was titrated with either ammonium chloride, L-glutamine, NAD^+, NADH, $NADP^+$, or NADPH dissolved in the same buffer (50 mM potassium phosphate, 1 mM DTT, pH 7.2) at 1.5–4 mM initial concentrations in the injection syringe. Experiments designed to detect any heat of ionization associated with the buffer and NAD^+, NADH, $NADP^+$, or NADPH used 50 mM PIPES, HEPES, TES, or Tris buffers, 1.0 mM DTT, pH 7.2. For the study of protein-protein interactions, $AreA_{662}$ in the calorimetric cell (1.4 ml) at concentrations in the range 37.5–50 μM were titrated with NmrA at a concentration of 454 μM in the injection syringe. The heat evolved following each 10-μl injection was obtained from the integral of the calorimetric signal. The heat due to the binding reaction was obtained as the difference between the heat of reaction and the corresponding heat of dilution. Analysis of data was performed using Microcal Origin Software. $AreA_{662}$ is encoded by a fragment of the *areA* gene subcloned into the *E. coli* expression vector pRSETB and has a heterologous N-terminal additional sequence that contains 6 histidine residues facilitating purification by immobilized metal affinity chromatography (see above). As a control we purified the protein encoded by the plasmid pRF12 (20) by using the same method as $AreA_{662}$ because it has the same N-terminal heterologous extension. When this protein was used in the ITC cell at a concentration of 35 μM, no heat exchange above base-line values was observed when NmrA was titrated into the protein solution. This control demonstrates that the heat exchange seen when NmrA is titrated into $AreA_{662}$ in the ITC cell was due to a specific interaction between NmrA and $AreA_{662}$.

Differential Scanning Calorimetry—Differential scanning calorimetry measurements on NmrA were made using Microcal VP-DSC or MCS instruments at a scan rate of 1 °C per min and a protein concentration of 17.3 (VP-DSC) or 108 μM (MCS). Protein was dialyzed in 50 mM KPO_4, pH 6.6, 1 mM DTT, and the dialysis buffer was retained to dissolve ligands, to dilute proteins, and for base-line controls. DSC experiments were repeated with addition of 3 mM putative effector (NAD^+, NADH, $NADP^+$, and NADPH) under otherwise identical conditions. Deconvolution analysis was performed using the non-two-state model using the Microcal Origin software.

Protein Crystallization and Structure Determination—The NmrA-$NADP^+$ complex was crystallized in form A (trigonal, space group $P3_221$, one molecule per asymmetric unit) using the conditions described previously (4, 5). X-ray data were collected at European Synchrotron Radiation Facility, Grenoble, France, on beamline ID29 using a wavelength of 0.99187 Å. The crystals were flash-frozen using 20% (v/v) glycerol as a cryoprotectant prior to data collection and maintained at 100 K. Data indexing/integration and merging were carried out using DENZO and SCALEPCK, respectively (21). Structure refinement used CNS (22), whereas model building was carried out using O (23) on an SGI Octane2 work station. The native NmrA coordinates (Protein Data Bank code 1K61) were used for rigid body refinement, followed by simulated annealing and positional and individual B-factor refinement. Data collection and refinement statistics are shown in Table IV. Figures of molecular models were created using VMD (24).

Energy Minimization of NmrA Dinucleotide Complexes—Minimization was carried out using the program NAMD2 (25) utilizing the CHARMM22 force field. NADH was initially placed in the same position as NAD^+ as observed from the crystal structure with NmrA (5). The system was then subjected to conjugate gradient minimization in the presence of water (coordinates obtained from the crystal structure). The very similar structures of NmrA seen in different crystal forms indicated a relatively rigid conformation for the protein, and hence the NAD(P)H-binding site was fixed except for the following key residues: His-37, Lys-131 Gly-151, Tyr-153, Asn-156, and Tyr-276. As a control, NAD^+ was also subjected to the same protocol.

RESULTS

NmrA Discriminates between Oxidized Dinucleotides and Their Reduced Forms—Purified NmrA was used in microcalorimetry experiments to quantify any interaction with NAD^+, $NADP^+$, NADH, and NADPH in HEPES, phosphate, PIPES, TES, and Tris buffers. The results of an ITC analysis (see Tables I–III) showed that NmrA was able to bind exothermically with 1:1 stoichiometry and moderate affinity to oxidized

[1] The abbreviations used are: DTT, dithiothreitol; DSC, differential scanning calorimetry; ITC, isothermal titration calorimetry; SDR, short-chain dehydrogenase reductase; PIPES, 1,4-piperazinediethanesulfonic acid; TES, 2-{[2-hydroxy-1,1-bis(hydroxymethyl)ethyl]amino}ethanesulfonic acid.

TABLE I

Thermodynamic parameters for the binding of NmrA to AreA$_{662}$ as determined by ITC at 25 °C

The binding of NmrA to AreA$_{662}$ was measured in phosphate buffer by ITC at the concentrations indicated. Shown are the values for n, the stoichiometry of binding; K_D, the equilibrium dissociation constant; ΔH_{obs}, the observed enthalpy; and ΔS^0, the standard entropy change for single site binding. The c values fall within the range 1–1000 that allows the isotherms to be accurately deconvoluted to derive K values (41).

[NmrA][a]	[AreA][b]	n	K_D	ΔH_{obs}	ΔS^0	c[c]
μM			μM	*kcal mol^{-1}*	*cal K^{-1} mol^{-1}*	
454	50	0.97 (±0.003)	0.28 (±0.02)	16.2 (±0.08)	84.5	173
454	50	0.99 (±0.002)	0.25 (±0.02)	15.5 (±0.07)	82.3	198
454	37.5	0.98 (±0.001)	0.26 (±0.01)	15.9 (±0.03)	83.4	141

[a] Protein concentration in injection syringe.
[b] Protein concentration in ITC cell.
[c] [NmrA] × K_A × n (the stoichiometry parameter).

dinucleotides with an average K_D in the region of 47 and 82 μM for NAD^+ and $NADP^+$, respectively. No binding of the reduced forms could be detected.

The ITC results were confirmed by differential scanning calorimetry (DSC) experiments (using a phosphate buffer) showing the effects of oxidized and reduced dinucleotides on the thermal stability of NmrA in solution under similar conditions (see Fig. 1). In the absence of added ligand, NmrA undergoes an endothermic thermal unfolding transition with $T_m \approx 48.5$ (±0.5) °C and mean enthalpy, $\Delta H = 670$ (±50) kJ mol^{-1}. Although the unfolding transition is irreversible under these conditions, the ratio of calorimetric to van't Hoff enthalpies, $\Delta H_{cal}/\Delta H_{VH} = 1.05$ (±0.12) is consistent with cooperative unfolding of a monomeric protein unit.

Addition of 3 mM NAD^+ or $NADP^+$ raises the T_m by about 4 °C, whereas the same concentration of reduced dinucleotides has only a marginal effect ($\delta T_m \approx 0.5$–1 °C). For a ligand that binds to the native (folded) state of a protein, the increase in T_m can be related to the dissociation constant (K_L) and concentration of ligand, [L], as shown in Equation 1,

$$\delta T_m/T_m = (RT_{m0}/\Delta H_{unf,0})\cdot\ln(1 + [L]/K_L) \quad \text{(Eq. 1)}$$

in which $\delta T_m = T_m - T_{m,0}$ is the change in unfolding transition temperature; R is the gas constant, and $\Delta H_{unf,0}$ is the unfolding enthalpy of the protein in the absence of ligand (26, 27). By using the data from DSC in the presence and absence of ligand with [L] = 3 mM, this expression gives estimates for $K_L \approx 0.15$ (±0.08) and 0.37 (±0.07) mM for NAD^+ and $NADP^+$, respectively, compared with much weaker values of 4.8 (±2.7) and 7.2 (±1.1) mM for NADH and NADPH under the same conditions. This is consistent with the more direct calorimetric titration data and shows clear discrimination in binding affinities for the oxidized and reduced forms of these ligands. It must be borne in mind that the DSC data relate to ligand binding at higher temperatures in the region of T_m where ligand binding affinities will be weaker compared with those determined by ITC at 25 °C. These ligand binding properties suggest the possibility that the binding of NAD^+ may modulate some aspect of the *in vivo* activity of NmrA. We are currently engaged in experiments to test this possibility.

Binding of NAD^+ and $NADP^+$ to NmrA Is Associated with Proton Uptake and Release—The ΔH_{obs} values given in Table IV are the observed enthalpy changes. These values include any heats of ionization that may be associated with the buffers and the reactants. The possibility that the ΔH_{obs} contains a component arising from heats of ionization can be checked by plotting ΔH_{obs} against the ionization enthalpies of the buffers used. Fig. 2 shows ΔH_{obs} plotted against the ionization enthalpies, ΔH_i, of the HEPES, PIPES, TES, and Tris buffers. These plots indicate that NAD^+ binding is associated with proton release, and $NADP^+$ binding is associated with proton uptake. The ΔH_{obs} values for NAD^+ and $NADP^+$ in phosphate buffer do not fit the trend of the plots shown in Fig. 2. The reason for this may be because the Rossmann fold has within it a pyrophosphate-binding site, and it is conceivable that phosphate can bind poorly to this site thereby acting as a weak inhibitor.

Structure of NmrA Complexed with $NADP^+$ and Modeling Studies of $NAD(P)^+$/NAD(P)H Discrimination—As a follow up to the calorimetry work that showed NmrA does not discriminate between NAD^+ and $NADP^+$ yet does in respect to oxidized/reduced nicotinamide adenine dinucleotides, we undertook structural studies in order to rationalize such observations at the molecular level. First, the crystal structure of NmrA complexed with $NADP^+$ was determined and refined to 1.7 Å resolution (Protein Data Bank code 1PDS). From the omit map shown in Fig. 3*A*, the $NADP^+$-binding site is clear and is positioned in a similar overall location to NAD^+ (5) yet with a significant difference in conformation for the adenosine fragment of the molecule (Fig. 3*C*). A number of hydrogen-bonding interactions occur between the protein and the NMN fragment of $NADP^+$ including Tyr-153 nitrogen to the nicotinamide oxygen, Gln-17 main-chain nitrogen to the 1 phosphate, and Arg-16 guanidinium to the 2 phosphate group. Further contacts with the nicotinamide include van der Waals interactions with Met-113 and ring stacking with the side chain of Tyr-153. Many of these interactions are the same as seen for the complex of NAD^+ with NmrA. There are, however, clear conformational differences between NAD^+ and $NADP^+$ in the adenosine portion of the dinucleotides. In the crystal structure of NAD^+ complexed with NmrA, the glycosidic bond of adenine, lies in the *anti* conformation and is set at 0° allowing the ring to make close stacking interactions with the side chain of His-37. $NADP^+$ adopts a different adenine ring conformation to NAD^+ due to the presence of the 2′-phosphate and in the complex with NmrA has the glycosidic bond of adenine residing at 91°; nevertheless, an equivalent ring stacking interaction of the adenine ring with the side chain of His-37 is maintained by flipping the latter by ~180° as shown in Fig. 3*C*. In addition, there is a movement of the adenosine ribose via a rotation of ~70° about the C-5′–O-5′ bond relative to NAD^+, shifting it toward residue Gln-84. The different adenine ring position in $NADP^+$ compared with NAD^+ leads to the loss of a hydrogen bond to the Thr-82 side-chain hydroxyl. However, the 2′-phosphate of $NADP^+$ makes interactions to the side-chain hydroxyl of Thr-14 via a water molecule.

Preliminary modeling studies have been used to assess structural features in NmrA that could contribute to the putative redox sensing mechanism, in particular as to why the protein binds NAD(P)H with low affinity compared with $NAD(P)^+$. Energy minimization of NmrA using NAMD2 indicates differences in the final conformation of NADH relative to NAD^+ in the NmrA-binding site, such that the nicotinamide ring of NADH has been displaced from its starting position. NAD^+ was found to be maintained in the same state as the crystal structure. The reduced nicotinamide has two different puckered conformers, both of which give steric clashes between

TABLE II
Thermodynamic parameters for the binding of NmrA to NAD^+ as determined by ITC at 25 °C

The binding of NmrA to NAD^+ was measured in the buffers shown by ITC at the concentrations indicated. The ±S.D. error estimates are as determined by the fitting software for individual experiments. Shown are the values for n, the stoichiometry of binding; K_D, the equilibrium dissociation constant; ΔH_{obs}, the observed enthalpy; and ΔS^0, the standard entropy change for single site binding. The c values fall within the range 1–1000 that allows the isotherms to be accurately deconvoluted to derive K values (41).

NAD^+	Buffer									
	Phosphate		PIPES		HEPES		TES		Tris	
[NmrA] μM[a]	80	80	110	110	104	104	157	134	83	83
[L] mM[b]	2.0	1.5	3.0	3.0	3.2	3.2	3.0	3.0	1.9	1.9
n	1.0 ± 0.02	1.0 ± 0.02	0.96 ± 0.01	1.09 ± 0.01	0.92 ± 0.03	0.90 ± 0.01	1.08 ± 0.02	1.02 ± 0.02	1.07 ± 0.05	1.02 ± 0.04
K_D (μM)	71 ± 3	68.9 ± 3	35 ± 1	31 ± 0.1	35 ± 0.8	35 ± 0.1	44 ± 2.6	48 ± 3.28	54 ± 4.8	58 ± 5.3
ΔH_{obs} (kcal mol^{-1})	−7.01 ± 0.2	−7.01 ± 0.14	−14.3 ± 0.02	−13.7 ± 0.09	−13.9 ± 0.59	−15.0 ± 0.12	−18.0 ± 0.3	−19.0 ± 0.55	−19.5 ± 1	−20.0 ± 1
ΔS^0 (K^{-1} mol^{-1})	−4.7	−4.6	−27.4	−27.3	−29.27	−30.67	−41.03	−44.09	−45.75	−48.37
c[c]	1.1	1.1	3.1	3.6	3.0	3.0	3.5	2.8	1.5	1.4

[a] NmrA concentration in the ITC cell.
[b] Nucleotide concentration in the injection syringe.
[c] c = [NmrA] × K_A × n (the stoichiometry parameter).

TABLE III
Thermodynamic parameters for the binding of NmrA to $NADP^+$ as determined by ITC at 25 °C

The binding of NmrA $NADP^+$ was measured in the buffers shown by ITC at the concentrations indicated. The ±S.D. estimates are as determined by the fitting software for individual experiments. Shown are the values for n, the stoichiometry of binding; K_D, the equilibrium dissociation constant; ΔH_{obs}, the observed enthalpy; and ΔS^0, the standard entropy change for single site binding. The c values fall within the range 1–1000 that allows the isotherms to be accurately deconvoluted to derive K values (41).

$NADP^+$	Buffer									
	Phosphate		PIPES		HEPES		TES		Tris	
[NmrA] μM[a]	184	220	110	110	163	163	157	134	83	83
[L] mM[b]	2.0	2.0	3.0	3.0	3.0	3.0	3.0	3.0	1.5	1.5
n	1.0 ± 0.01	1.1 ± 0.01	1.0 ± 0.02	1.0 ± 0.02	1.0 ± 0.01	1.0 ± 0.01	1.0 ± 0.02	1.0 ± 0.02	1.0 ± 0.02	1.0 ± 0.02
K_D (μM)	100 ± 2	119 ± 1.5	60 ± 1.7	58 ± 2.2	103 ± 1.2	105 ± 1.3	107 ± 1.7	109 ± 0.3	34 ± 1.6	32 ± 2.1
ΔH_{obs} (kcal mol^{-1})	−12.0 ± 0.1	−11.3 ± 0.1	−28.7 ± 0.05	−28.1 ± 0.05	−24.3 ± 0.19	−24.0 ± 0.12	−22.6 ± 0.36	−22.7 ± 0.49	−12.0 ± 0.33	−12.0 ± 0.34
ΔS^0 (K^{-1} mol^{-1})	−22	−20	−76.97	−74.79	−63.23	−62.51	−57.63	−58.3	−19.86	−19.67
c[c]	1.8	1.9	1.8	1.9	1.7	1.7	1.5	1.2	2.5	2.6

[a] NmrA concentration in the ITC cell.
[b] Nucleotide concentration in the injection syringe.
[c] [NmrA] × K_A × n (the stoichiometry parameter).

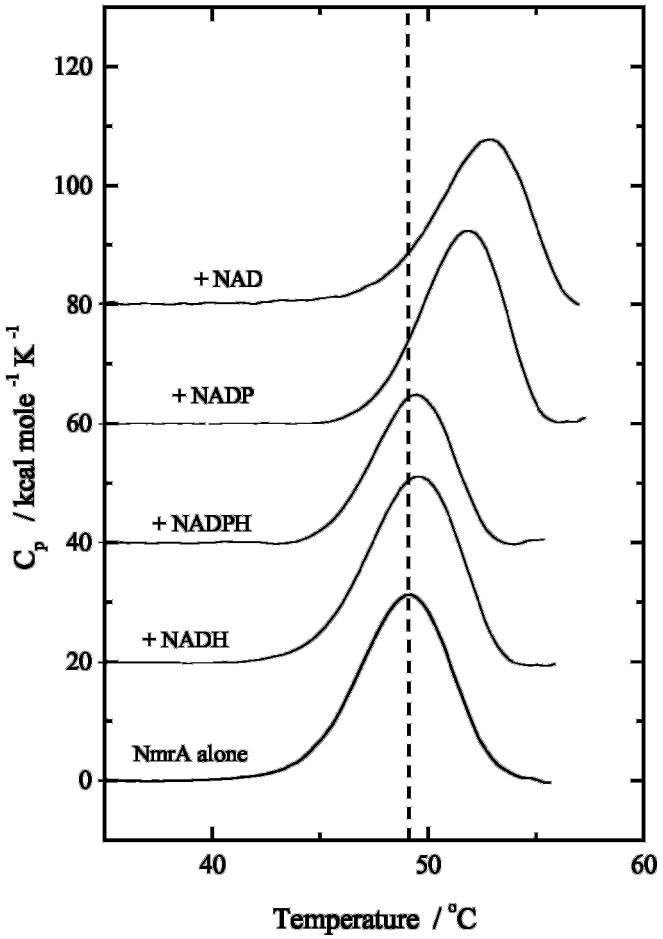

FIG. 1. **DSC data (offset for clarity) comparing the thermal unfolding transitions of NmrA (17 μM) in the presence and absence of 3 mM oxidized or reduced dinucleotides.** Heat capacity data are corrected for instrumental (buffer) base line, and concentration was normalized (1 cal = 4.184 J). The *dashed line* indicates the T_m (48.5 °C) of free protein and highlights the relatively large increase in thermal stability in the presence of NAD^+ (52.5 °C) or $NADP^+$ (51.6 °C), compared with the much smaller effects with NADH (49.3 °C) or NADPH (49.4 °C).

TABLE IV
Statistics for crystallographic structure determination
Outer shell data are given in parentheses.

Data collection details	
Data set	NmrA-$NADP^+$
Data collection site	ERSF ID-29
Wavelength (Å)	0.993
Unit cell (a, b, c in Å)	76.4, 76.4, 104.2
Resolution range (Å)	30.0–1.7 (1.76–1.70)
Observations	387,915
Unique reflections	39,254 (3848)
Completeness (%)	100.0 (100.0)
$I/\sigma I$	19.39 (1.43)
R_{merge} [a]	0.092 (0.582)
Refinement statistics	
Resolution range (Å)	30.0–1.7
Unique reflections (working/test)	37235,1955
R-factor[b] (R-working/R-free)	0.174, 0.177/0.227
No. atoms (protein/solvent/ion)	2558/509/8
Root mean square bond length deviation (Å)	0.0086
Root mean square bond angle deviation (°)	1.47
Mean B-factor (Å^2)	24.7

[a] $R_{merge} = \Sigma|I - \langle I\rangle| / \Sigma\langle I\rangle$.
[b] R-factor $= \Sigma|F_o - F_c| / \Sigma F_o$.

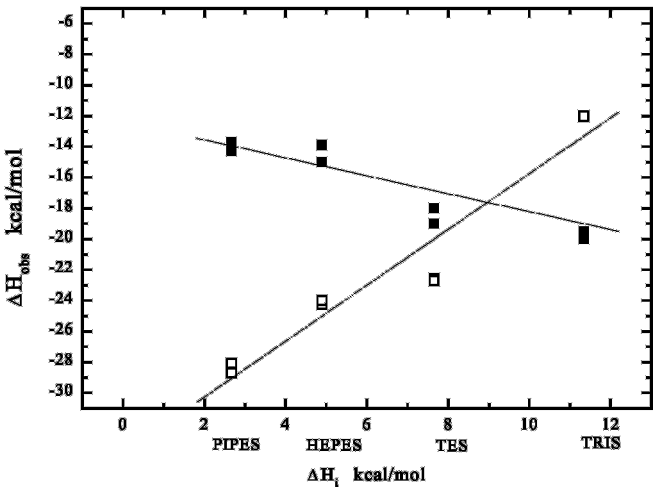

FIG. 2. **Linear regression analysis of a plot of ΔH_{obs} *versus* the heat of ionization, ΔH_i, of the buffers PIPES, HEPES, TES, and Tris.** Data from two independent experiments are shown. The *closed squares* for NAD^+ binding and the *open squares* for $NADP^+$ binding are generated from the data shown in Tables I–III.

the additional hydrogen atoms present at the C4-position and the backbone oxygen atom in residue Gly-151 as well as the Tyr-276 side-chain hydroxyl group. The loss of aromaticity of the nicotinamide ring in NAD(P)H is also likely to weaken binding as ring stacking interactions with the side chain of Tyr-153 will be attenuated (28). There is also a distortion of the hydrogen bonding interactions of the amide group in the puckered conformers with the side chain of Asn-156. A further factor is the positive charge in the nicotinamide ring of $NAD(P)^+$ which is delocalized causing the outer hydrogens to have a partial charge (29). The polar nature of these hydrogens may allow weak electrostatic interactions between $NAD(P)^+$ and the backbone oxygen atoms of residues Gly-151 and Ala-150 in NmrA. Similar interactions of this nature are observed with other protein ligand complexes (30). However, in NADH the C-4 hydrogen atoms can no longer partake in such an interaction, which results in a steric clash with the backbone oxygen of Gly-151, when in the planar conformation (Fig. 3*D*). By using the ligand docking program G.O.L.D (31), the experimentally determined binding position of the nicotinamide mononucleotide portion of NAD^+ and $NADP^+$ in NmrA could be accurately reproduced. G.O.L.D. also gave consistently lower fitness scores with NADH compared with NAD^+ and docked NADH in a displaced position from NAD^+.

In the case of nicotinamide adenine dinucleotide- binding enzymes in general, there is normally high selectivity for NAD^+ relative to $NADP^+$ and vice versa. Whereas this discrimination cannot be put down to a particular common set of residues, nevertheless "fingerprint" interactions for NAD^+ (a side-chain carboxylate interacting with the adenosine ribose hydroxyls) and for $NADP^+$ (an arginine facing the adenine plane and interacting with the pyrophosphate) have been identified (32, 33). Unusually dihydrodipicolinate reductase shows a relatively low discrimination between NADH and NADPH of 4-fold, and in this case the carboxylate of Glu-38 interacts with the adenosine ribose hydroxyls of NADH but does not make this interaction in the NADPH complex (34). The dihydrodipicolinate reductase NADPH complex has an interaction that is not present in the NADH complex involving Arg-39. In this case the arginine hydrogen bonds to the 2′-phosphate rather than the pyrophosphate group, which is characteristic of the normal fingerprint interaction for $NADP^+$. $NADP^+$-specific SDRs have a pair of conserved basic residues (Lys-17 and Arg-39 in carbonyl reductase) that have been suggested as

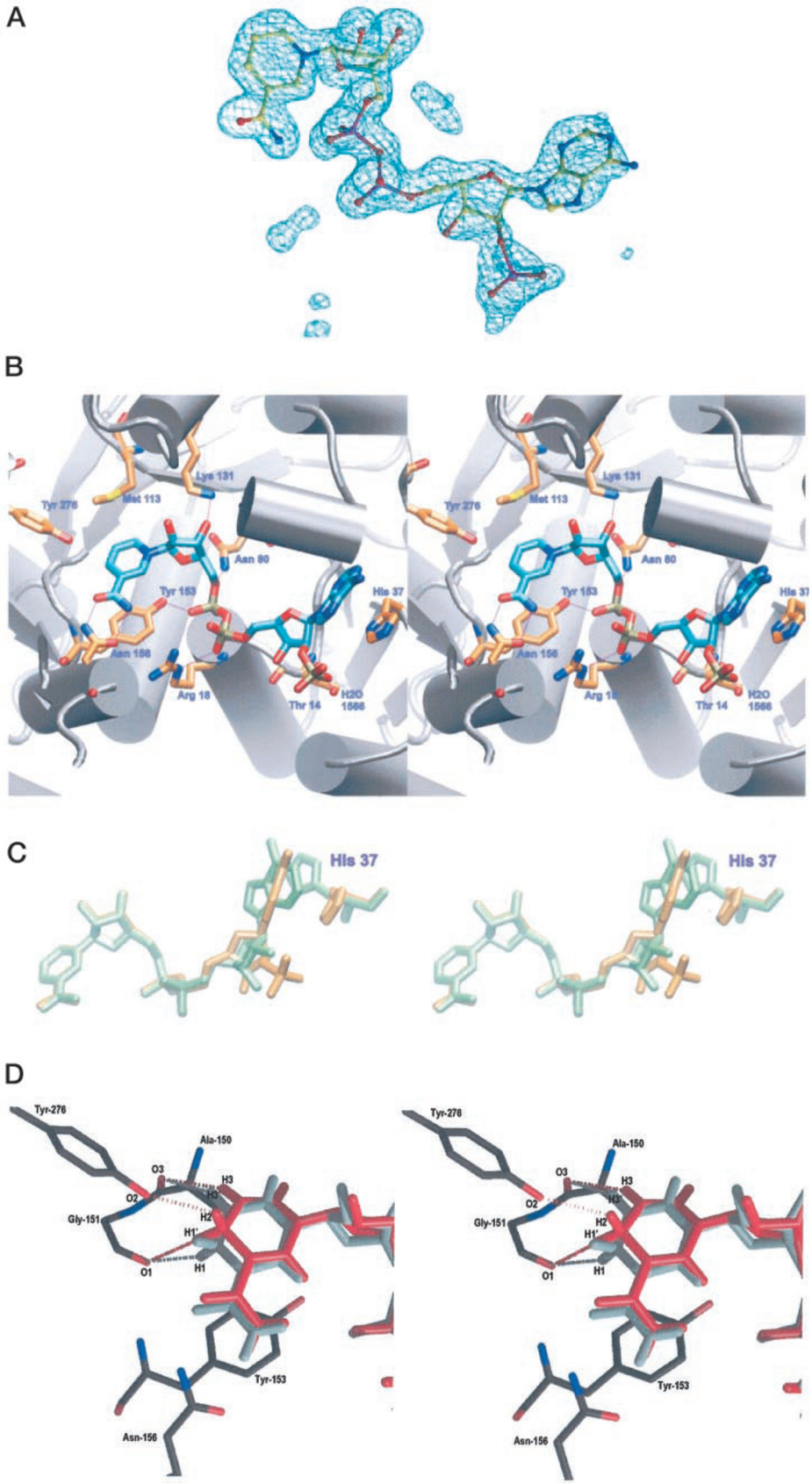

FIG. 3. *A*, omit map for $NADP^+$ in its binding site on NmrA. The map is contoured at 2.7σ and shows clear density for the ligand. *B*, interaction of $NADP^+$ with NmrA. Stereo diagram with key residues indicated. Hydrogen bond contacts (in *purple*) are shown between atoms. NmrA is depicted in schematic format. *C*, comparison of the conformations of $NADP^+$ and NAD^+ when bound to NmrA. Stereo diagram with NAD^+ shown in *green* and $NADP^+$ in *orange*. *D*, NAMD2 minimization of NADH. Stereo diagram showing the modeling results obtained using NAMD2 with NADH. Protein hydrogen atoms and water molecules have been omitted for clarity. The starting conformation of NADH is indicated in *gray*, and the minimized structure is shown in *red*, and the conformation of the protein is shown as in the minimized structure. Key interactions are indicated with *dashed lines*, and atom labels define the following bond lengths: O-1—H-1, 2.45 Å; O-1—H-1′, 3.11 Å; O-2—H-2, 2.66 Å; O-3—H-3, 2.65 Å; O-3–H3′, 2.59 Å. Overall, there was very little difference in the conformation of these residues before and after modeling, except in the case of Tyr-276, which moved slightly by 0.73 Å. Hence, no bond has been shown between this and the starting conformation of NADH.

providing the recognition for this dinucleotide by interacting with the 2′-phosphate (35). Interestingly in NmrA, which does not discriminate between NAD^+ and $NADP^+$, there are no homologous residues to these positions in carbonyl reductase. Also, significantly, for NmrA both fingerprint interactions for NAD^+ and $NADP^+$ are absent. The observed rearrangement of His-37 allows NmrA to bind either NAD^+ or $NADP^+$ by accommodating the differing conformations of the adenine ring moieties of these two dinucleotides.

NmrA Binds to a C-terminal Fragment of AreA—Previous

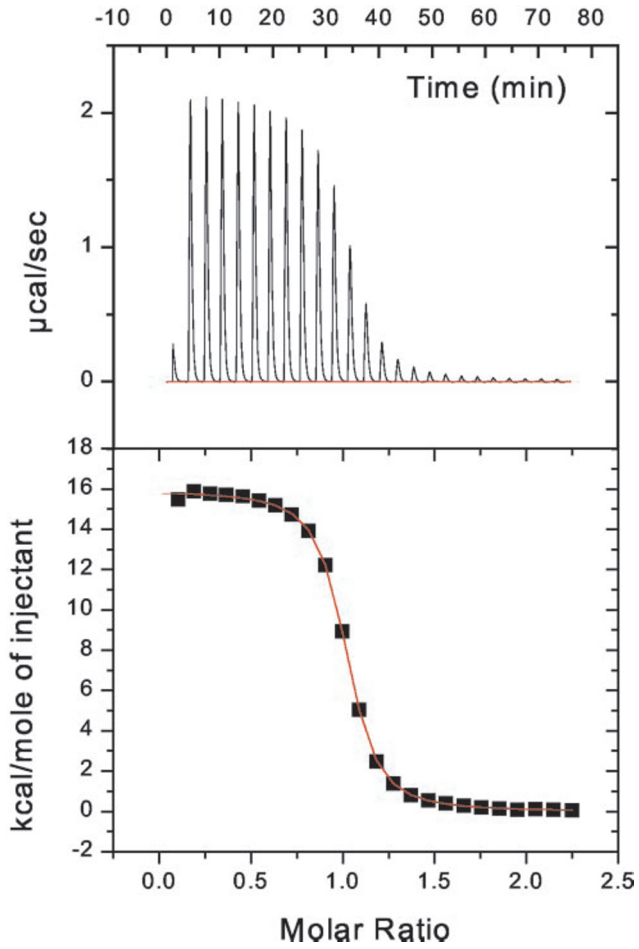

FIG. 4. **Typical ITC data for the endothermic binding of NmrA to AreA at 25 °C.** *Upper panel*, heat uptake upon injection (1 × 2 µl and 24 × 10 µl) of NmrA (454 µM) into the calorimetric cell (1.4 ml) containing $AreA_{662}$ at 37.5 µM. Heat pulses in the absence of AreA (not shown) were negligible. *Lower panel*, integrated heat pulses, normalized per mol of injectant, giving a differential binding curve that is adequately described by a single-site binding model.

work with NMR1 showed that *in vitro* it interacted with the C-terminal region of NIT2 (17). In order to characterize the kinetics of any interaction between NmrA and the C-terminal region of AreA, we deleted the N-terminal 662 amino acids of AreA to produce a small C-terminal fragment (designated $AreA_{662}$) for this analysis (see "Experimental Procedures"). This C-terminal fragment of AreA contains the zinc finger region and was able to bind to the *niaD* promoter (36) *in vitro* in electrophoretic mobility shift assay experiments (data not shown).

NmrA and $AreA_{662}$ were purified in bulk and used in ITC experiments to determine whether they interacted with one another. We carried out experiments in which NmrA in the injector syringe was titrated into $AreA_{662}$ in the reaction cell. The results of these experiments are shown in Tables I–III, where it can be seen that NmrA and $AreA_{662}$ interacted endothermically with a 1:1 stoichiometry and an average K_D of 0.26 µM. Fig. 4 shows typical results of the titration of NmrA into $AreA_{662}$.

In order to determine whether nucleotide binding was affected by the interaction of AreA with NmrA, we carried out experiments in which NAD^+, NADH, or $NADP^+$ in the injector syringe was titrated into an approximately equimolar mixture of NmrA and $AreA_{662}$. The resulting thermograms were not significantly different from those observed in the absence of AreA, indicating that formation of the NmrA-AreA complex does not inhibit (oxidized) nucleotide binding nor does it affect the discrimination between oxidized and reduced forms. This is consistent with the structural studies that show that the nucleotide-binding site in NmrA is distant from the putative AreA interaction region.

NmrA Is Unable to Bind the Nitrogen Metabolite Repression Signal Molecules Ammonium or Glutamine—The fact that NmrA can bind NAD^+, $NADP^+$, and $AreA_{662}$ implies that the protein is in a native state able to bind physiological ligands after our purification protocol. We used ITC to probe the ability of NmrA to bind the nitrogen metabolite repression signal molecule glutamine in a binary complex and in a ternary complex with $AreA_{662}$. We were unable to detect any significant heat of binding when glutamine was added to a solution of $AreA_{662}$ (40 µM) or NmrA. Also when the ITC cell contained NmrA (44.6 µM) previously titrated with $AreA_{662}$ (312 µM), no heat of binding was observed when glutamine was titrated into the NmrA-AreA complex. We also used circular dichroism and fluorescence emission spectroscopy as independent techniques to probe the ability of NmrA to bind ammonium or glutamine in a binary complex; however, no conformational changes and no binding could be detected (data not shown).

DISCUSSION

We have quantified for the first time the ligand binding properties of NmrA, a protein that plays a major role in the signal transduction pathway controlling nitrogen metabolite repression in microbial eukaryotes. Calorimetry reveals that NmrA does not discriminate between NAD^+ and $NADP^+$ but can effectively discriminate between the oxidized and reduced forms. Structure determination of the complex of NmrA with $NADP^+$ and comparison with the previous NAD^+ complex reveal that repositioning of His-37 allows the significantly different conformations of the adenosine moiety of the two dinucleotides to be accommodated within the same binding site. Additionally, it may be noted that some structural features that have been ascribed to the $NAD^+/NADP^+$ discrimination in SDRs have been lost in NmrA (35). Because a range of mutations are needed to change $NAD^+/NADP^+$ selectivity (32), it would seem that the ancestral ability of the SDR fold in NmrA to discriminate between NAD^+ and $NADP^+$ is unlikely to have been lost as the result of a single mutation that has become fixed through a stochastic event. The unusual ability of NmrA to bind NAD^+ and $NADP^+$ with equal affinity is more likely to be the result of evolutionary selection and implies that it may be of physiological importance. Similarly the ability of NmrA to discriminate between $NAD(P)^+$ and NADPH may have a biological function. The molecular basis for this discrimination between oxidized and reduced dinucleotides has been investigated by studies that show the reduced nicotinamide ring produces steric clashes and loss of aromatic ring stacking and electrostatic interactions with NmrA. Calorimetry also demonstrates that NmrA is able to bind to $AreA_{662}$, a C-terminal fragment of AreA, a protein that plays an essential role in the positive control of transcription, with a 1:1 stoichiometry and an apparent K_D of 0.26 µM.

The signal transduction pathway involving NmrA has been implicated in monitoring the intracellular levels of the nitrogen metabolite repression signal molecule glutamine (37). However, CD spectroscopy, fluorescence, and calorimetry provide no evidence that NmrA can recognize ammonium or glutamine in either a binary complex or a ternary complex with $AreA_{662}$. The inability of NmrA to bind ammonium or glutamine in a binary complex or a ternary complex with $AreA_{662}$ may mean that NmrA is not involved in the glutamine sensing signal transduction pathway that controls wild-type nitrogen metabolite repression. Glutamine-binding sites may exist on other

regions of AreA or only in a higher order complex when additional components are present.

We note that two radically different models for the ability of NmrA to modulate the activity of AreA can be envisaged. NmrA may interact directly with AreA while it is complexed with DNA and disrupt its interaction with pathway-specific transcription-regulating proteins or the accessory transcription apparatus. On the other hand, NmrA may exert its affect by controlling the access of AreA to its target promoters by either a direct or indirect route. The direct route could involve occlusion of the zinc finger region (17), or it could act indirectly by controlling the rate of entry of AreA into the nucleus. The moderate affinity for the oxidized dinucleotides (average value 65 μM) means that in order to have a substantial proportion of the population in a binary complex with NAD^+/$NADP^+$, NmrA must be in an environment with oxidized nucleotides in the high micromolar range. The free intracellular and nuclear concentrations of oxidized and reduced nucleotides in *A. nidulans* are not known, and their determination is beyond the scope of this current study. However, overall intracellular concentrations of 1 mM for NAD^+ plus NADH have been reported in the microbial eukaryote *Saccharomyces cerevisiae* (38), and there is no reason to assume that *A. nidulans* will differ dramatically. If this situation is reflected in *A. nidulans*, then a dinucleotide signal recognition role for NmrA may be restricted to the cytosol where NmrA is most likely to encounter the highest concentrations of NAD^+/$NADP^+$. If NmrA functions to control the access of AreA to the nucleus, the binding of oxidized dinucleotides could modulate this ability.

The ligand binding properties of NmrA show some interesting parallels to those of the CtBP class of transcriptional corepressor. The latter proteins are related to a metabolic enzyme, in the case of CtBP, sharing a high degree of amino acid sequence homology with NAD^+-dependent 2-hydroxy acid dehydrogenases. Whereas NmrA shares no sequence identity with dehydrogenases, it nevertheless has a three-dimensional structure related to the SDR superfamily. CtBP proteins are widespread and are conserved between vertebrates and invertebrates being involved in transcriptional pathways important for development, cell cycle regulation, and transformation (39, 40). CtBP binding to cellular and viral transcriptional repressors is regulated by NAD^+ and NADH, with NADH being 2–3 orders of magnitude more effective. It is proposed that the ability of CtBP to detect changes in nuclear NAD^+/NADH ratio allows it to serve as a redox sensor for transcription (39). In the case of NmrA, however, NAD^+ binds more effectively than NADH, and it interacts with a wide domain GATA-type transcription activator rather than a transcription repressor. Further studies of the AreA/NmrA transcriptional regulatory system including investigations into the role of NAD^+ will allow more detailed understanding of potential relationships with other transcription factors that are thought to have roles in redox sensing.

Acknowledgments—The Biological Microcalorimetry facility in Glasgow is funded jointly by the Biotechnology and Biological Sciences Research Council and Engineering and Physical Sciences Research Council. We thank Elaine Cairns for technical assistance.

REFERENCES

1. Wilson, R. A., and Arst, H. N., Jr. (1998) *Microbiol. Mol. Biol. Rev.* **62,** 586–596
2. Dunn-Coleman, N. S., Tomsett, A. B., and Garrett, R. H. (1979) *J. Bacteriol.* **139,** 697–700
3. Andrianopoulos, A., Kourambas, S., Sharp, J. A., Davis, M. A., and Hynes, M. J. (1998) *J. Bacteriol.* **180,** 1973–1977
4. Nichols, C. E., Cocklin, S., Dodds, A., Ren, J., Lamb, H., Hawkins, A. R., and Stammers, D. K. (2001) *Acta Crystallogr. Sect. D Biol. Crystallogr.* **57,** 1722–1725
5. Stammers, D. K., Ren, J., Leslie, K., Nichols, C. E., Lamb, H. K., Cocklin, S., Dodds, A., and Hawkins, A. R. (2001) *EMBO J.* **20,** 6619–6626
6. Thoden, J. B., Wohlers, T. M., Fridovich-Keil, J. L., and Holden, H. M. (2000) *Biochemistry* **39,** 5691–5701
7. Jornvall, H., Persson, B., Krook, M., Atrian, S., Gonzalez-Duarte, R., Jeffery, J., and Ghosh, D. (1995) *Biochemistry* **34,** 6003–6013
8. Rutter, J., Reick, M., Wu, L. C., and McKnight, S. L. (2001) *Science* **293,** 510–514
9. Grove, G., and Marzluf, G. A. (1981) *J. Biol. Chem.* **256,** 463–470
10. Davis, M. A., and Hynes, M. J. (1987) *Proc. Natl. Acad. Sci. U. S. A.* **84,** 3753–3757
11. Fu, Y. H., and Marzluf, G. A. (1990) *Mol. Cell. Biol.* **10,** 1056–1065
12. Marzluf, G. A. (1997) *Microbiol. Mol. Biol. Rev.* **61,** 17–32
13. Platt, A., Langdon, T., Arst, H. N., Jr., Kirk, D., Tollervey, D., Sanchez, J. M., and Caddick, M. X. (1996) *EMBO J.* **15,** 2791–2801
14. Muro-Pastor, M. I., Gonzalez, R., Strauss, J., Narendja, F., and Scazzocchio, C. (1999) *EMBO J.* **18,** 1584–1597
15. DeBusk, R. M., and Ogilvie, S. (1984) *J. Bacteriol.* **160,** 493–498
16. Young, J. L., and Marzluf, G. A. (1991) *Biochem. Genet.* **29,** 447–459
17. Xiao, X., Fu, Y. H., and Marzluf, G. A. (1995) *Biochemistry* **34,** 8861–8868
18. Maniatis, T., Fritsch, E. F., and Sambrook, J. (1982) *Molecular Cloning: A Laboratory Manual*, Cold Spring Harbor Laboratory Press, New York
19. Lamb, H. K., Newton, G. H., Levett, L. J., Cairns, E., Roberts, C. F., and Hawkins, A. R. (1996) *Microbiology* **142,** 1477–1490
20. Lamb, H. K., Moore, J. D., Lakey, J. H., Levett, L. J., Wheeler, K. A., Lago, H., Coggins, J. R., and Hawkins, A. R. (1996) *Biochem. J.* **313,** 941–950
21. Otwinowski, Z., and Minor, W. (1996) *Methods Enzymol.* **276,** 307–326
22. Brunger, A. T., Adams, P. D., Clore, G. M., Delano, W. L., Gros, P., Grosse, K. R. W., Jiang, J. S., Kuszewski, J., Nilges, M., Pannu, N. S., Read, R. J., Rice, L. M., Simonson, T., and Warren, G. L. (1998) *Acta Crystallogr.* **54,** 905–921
23. Jones, T. A., Zou, J. Y., Cowan, S. W., and Kjeldgaard, M. (1991) *Acta Crystallogr.* **47,** 110–119
24. Humphrey, W., Dalke, A., and Schulten, K. (1996) *J. Mol. Graph.* **14,** 33–38
25. Kale, L., Skeel, R., Bhandarkar, M., Brunner, R., Gursoy, A., Krawetz, N., Phillips, J., Shinozaki, A., Varadarajan, K., and Schulten, K. (1999) *J. Comput. Phys.* **151,** 283–312
26. Cooper, A., Nutley, M. A., and Wadood, A. (2000) in *Protein-Ligand Interactions: Hydrodynamics and Calorimetry* (Harding, S. E. and Chowdry, B. Z., eds) pp. 287–318, Oxford University Press, Oxford, UK
27. Cooper, A. (1999) in *Protein: A Comprehensive Treatise* (Allen, G., ed) Vol. 2, pp. 217–270, JAI Press Inc., Greenwich, CT
28. McGaughey, G. B., Gagne, M., and Rappe, A. K. (1998) *J. Biol. Chem.* **273,** 15458–15463
29. Levitt, M., and Perutz, M. F. (1988) *J. Mol. Biol.* **201,** 751–754
30. Klaholz, B., and Moras, D. (2002) *Structure* **10,** 1197–1204
31. Jones, G., Willett, P., Glen, R. C., Leach, A. R., and Taylor, R. (1997) *J. Mol. Biol.* **267,** 727–748
32. Carugo, O., and Argos, P. (1997) *Proteins* **28,** 29–40
33. Carugo, O., and Argos, P. (1997) *Proteins* **28,** 10–28
34. Reddy, S. G., Scapin, G., and Blanchard, J. S. (1996) *Biochemistry* **35,** 13294–13302
35. Tanaka, N., Nonaka, T., Nakanishi, M., Deyashiki, Y., Hara, A., and Mitsui, Y. (1996) *Structure* **4,** 33–45
36. Punt, P. J., Strauss, J., Smit, R., Kinghorn, J. R., van den Hondel, C. A., and Scazzocchio, C. (1995) *Mol. Cell. Biol.* **15,** 5688–5699
37. Morozov, I. Y., Galbis-Martinez, M., Jones, M. G., and Caddick, M. X. (2001) *Mol. Microbiol.* **42,** 269–277
38. Bakker, B. M., Overkamp, K. M., van Maris, A. J., Kotter, P., Luttik, M. A., van Dijken, J. P., and Pronk, J. T. (2001) *FEMS Microbiol. Rev.* **25,** 15–37
39. Chinnadurai, G. (2002) *Mol. Cell* **9,** 213–224
40. Schaeper, U., Boyd, J. M., Verma, S., Uhlmann, E., Subramanian, T., and Chinnadurai, G. (1995) *Proc. Natl. Acad. Sci. U. S. A.* **92,** 10467–10471
41. Wiseman, T., Williston, S., Brandts, J. F., and Lin, L. N. (1989) *Anal. Biochem.* **179,** 131–137